ChemPubSoc Europe

DOI: 10.1002/open.201800162

Open Access ChemistryOPEN Full Papers

Development and Application of Carbon-Layer-Stabilized, Nitrogen-Doped, Bamboo-Like Carbon Nanotube Catalysts in CO_2 Hydrogenation

Emőke Sikora,[a] Ádám Prekob,[a] Gyula Halasi,[b] László Vanyorek,*[a] Péter Pekker,[c] Ferenc Kristály,[d] Tamás Varga,[b] János Kiss,[e] Zoltán Kónya,[b] and Béla Viskolcz[a]

Nitrogen-doped, bamboo-like carbon nanotubes (BCNTs) were synthesized from butylamine by catalytic chemical vapor deposition (CCVD method). The nanotubes were oxidized by H_2SO_4/HNO_3 treatment and used to prepare calcium alginate gelled BCNT spheres. These beads were first carbonized and then Pd, Rh and Ni nanoparticles were anchored on the surface of the spheres. These systems were then applied as catalysts in CO_2 hydrogenation. The BCNT support was examined by Raman spectroscopy, dynamic light scattering (DLS) and X-ray photoelectron spectroscopy (XPS). The prepared catalysts were characterized by HRTEM and SEM. The oxidation pretreatment of BCNTs was successful, with the electrokinetic potential of the water-based dispersion of BCNTs measuring −59.9 mV, meaning the nanotube dispersion is stable. Pyridinic and graphitic types of incorporated nitrogen centers were identified in the structure of the nanotubes, according to the XPS measurements. The Pd-containing BCNT sphere catalyst was the most efficient in the catalytic studies. The highest conversion was reached on the Pd catalyst at 723 K, as well as at 873 K. The difference in the formation rate of CO was much less at 873 K between the Pd and Rh compared to the 723 K values. Accordingly, the application of Pd-containing BCNT/carbon-supported catalyst favored the generation of CO. However, the Ni-BCNT/carbon catalyst leads to the formation of CH_4 as the major product.

1. Introduction

Carbon nanotubes are promising catalyst support materials due to their high specific surface area and good mechanical[1–3] and thermal stabilities.[4] Functionalized carbon nanotubes can be produced via oxidation processes which makes them ideal binding sites for catalytically active metal ions. CNTs are suitable to be used in many areas of the electronics industry, such as in solar cells,[5] semiconductor devices[6] or for magnetic data storage.[7] Their exceptional mechanical properties can be exploited in composite production.[8–11] The alternative applications of carbon nanotubes include bulletproof materials or lightweight bicycle frames.[12]

However, CNTs do not contain micropores and therefore the catalysis can be more effective and more resistant to oxidation processes than the previously popular activated carbon. CNTs are widely used in several catalytic reactions such as hydrogenation as well as in the Fischer–Tropsch process.[13] Nanotubes have been proved useful in environmental remediation procedures.[14–15] Xiaoshu et al. prepared and used nanoscale zero-valent iron—multiwalled carbon nanotube (MWCNT) nanocomposites to remove Cr^{VI} from wastewater.[16] Wang et al. developed highly active electrocatalysts using nitrogen-doped bamboo-like carbon nanotubes.[17] Liao et al. synthesized Pd/C, Pt/C, Ni/CNT and Pd/CNT catalysts and tested them in the hydrogenation of nitrocyclohexene.[18] The most promising catalytic activity were achieved (97.6% conversion) in the case of 5 wt% Pd/CNT.[18] The Pd, Rh and Ni transition metals were selected for a detailed study of the catalytic activity used by a bamboo-like carbon nanotube (BCNTs) support. The BCNTs are special types of MWCNTs prepared from nitrogen-containing carbon compounds. BCNTs have defect sites, resulting from the incorporated nitrogen atoms, which makes high energy

[a] E. Sikora, Á. Prekob, Dr. L. Vanyorek, Prof. B. Viskolcz
Institute of Chemistry, University of Miskolc
3515 Miskolc Egyetemváros (Hungary)
E-mail: kemvanyi@uni-miskolc.hu

[b] Dr. G. Halasi, T. Varga, Prof. Z. Kónya
Department of Applied and Environmental Chemistry
University of Szeged
6720 Szeged (Hungary)

[c] P. Pekker
Research Institute of Biomolecular and Chemical Engineering
University of Pannonia
8200 Veszprém (Hungary)

[d] Dr. F. Kristály
Institute of Mineralogy and Geology, University of Miskolc
3515 Miskolc Egyetemváros (Hungary)

[e] Prof. J. Kiss
Reaction Kinetics and Surface Chemistry Research Group
University of Szeged
6720 Szeged (Hungary)

Supporting Information and the ORCID identification number(s) for the author(s) of this article can be found under: https://doi.org/10.1002/open.201800162.

absorption sites for catalytically active metal particles.[19,20] According to Li et al., the high electron affinity of incorporated nitrogen promotes the binding of Pt atoms to N-doped bamboo-like nanotubes.[21] Other carbon forms doped with P, P and S centers, namely hollow carbon polyhedrons and hierarchically porous carbon spheres, have also been employed as promising electrode and supercapacitor materials.[22–23] One of the most important features of N-doped nanotubes is the activation of the nitrogen-neighboring carbon atoms. The p–d hybridizations help to bind transition metals in a catalytically active form. Higher catalytic activity of N-doped bamboo-like nanotubes were detected in the hydrogenation reaction compared with undoped multiwalled nanotubes.[24] Additional benefits are the high number of edges of N-doped CNTs resulting from facile functionalization of carbon atoms at the edge.[19,20] Different oxidation state can be formed on the edge, namely carboxy, carbonyl and hydroxy groups. The carboxy and hydroxy groups can be deprotonated, thereby resulting in a negative electrokinetic (Zeta) potential of the BCNTs. The increased surface charges result in a more stable aqueous dispersion of the carbon nanotubes.

Considering the depletion of fossil energy sources, CO_2 hydrogenation to hydrocarbons is a potential means to convert carbon dioxide into fuels or other valuable products. In the last few years, more extensive research has been performed on CO_2 hydrogenation than ever before. Catalytic hydrogenation of carbon dioxide using hydrogen to produce renewable energy is considered as a possible way forward for the sustainable production of hydrocarbons, [25] carboxylic acids,[26] methanol,[27] and higher alcohols.[28] However, due to the high activation energy for the formation of C–C bonds, it is still a great challenge to produce hydrocarbons with relatively high selectivity. Modern techniques have made it possible to follow these processes with different methods such as NAP-XPS (near ambient pressure XPS),[27] NEXAFS (near-edge X-ray absorption fine structure),[30] photoelectrochemistry,[31] or photochemistry.[32] This research field is more than forty years old, and at that time oxide-supported noble metals as catalysts were frequently applied.[33] Nowadays, the aim of many researchers is to apply noble-metal-free catalysis.[34]

In the present work we report the preparation of strongly functioning catalyst, which can be easily recovered, and takes advantage of the beneficial properties of BCNTs. We compare the activity of different systems in the hydrogenation of CO_2, with emphasis on the effects of the anchored metal. We focused on the comparison of three similarly structured BCNT-based materials. The hydrogenation was ≈9 times higher at 723 K on the supported Pd sample compared to the Rh/BCNT. In the case of Ni/BCNT, selectivity towards methane was ten times higher (64%) than on the Pd/BCNT catalyst (6.8%). With the goal to avoid the use of noble metals and instead employ the much cheaper transition metals, the BCNT-based supported Ni catalysts are a good alternative in this reaction. At the same time, using BCNT as a support in heterogeneous catalysis including CO_2 hydrogenation provides the possibility to study the role of metals without metal/oxide-like support interactions.

2. Results and Discussion

2.1. Characterization of BCNTs

The morphology and tube diameters were examined by HRTEM. The micrographs of the bamboo-like structure of the nanotubes were shown on Figure 1a. The high resolution image indicated that a significant amount of graphene edges were found on the wall of the nanotube (Figure 1b). The outer diameters of the nanotubes were manually scaled using an ImageJ program. The distribution of nanotube diameters is shown in (Figure 1d). Based on the images, the diameter of the BCNTs was between 10 nm and 50 nm, the average value was 26.1 nm.

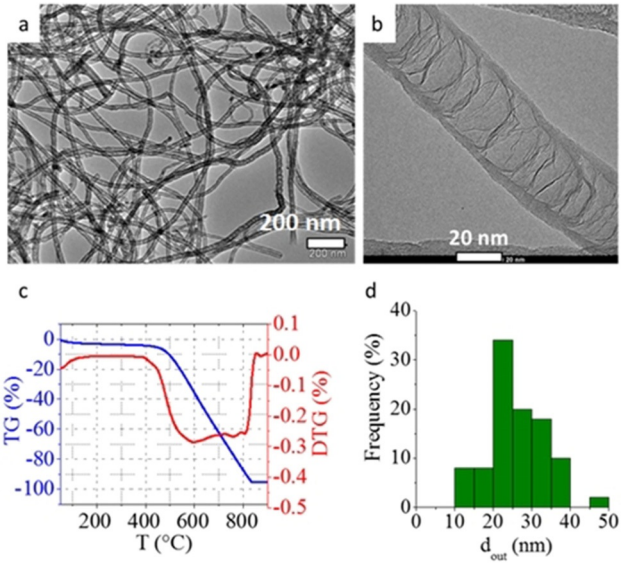

Figure 1. a, b) Typical TEM and HRTEM images of BCNTs, c) TG and DTG curves of nanotubes and d) size distribution of BCNT based on the TEM images.

The purity of the BCNTs was checked with thermogravimetric tests. Based on the TGA results, weight loss can be observed in the region of 700 K to 990 K which occurred due to the oxidation of the carbon (Figure 1c). The remaining mass contained residue which cannot be removed by the cleaning procedure. This is typically as a result of encapsulated Ni particles inside the BCNT. Based on the measurements, the carbon content of the sample was calculated to be 92.3 wt%.

Considering the XPS spectra, the deconvoluted N 1s spectral assignment of different types of incorporated nitrogen atoms are shown in Figure 2a. The binding energy of 398.4 eV indicated pyridinic N atoms and the peak at 401.2 eV was assigned to graphitic nitrogen. The binding energy at 402–405 eV was attributed to adsorbed nitrogen or nitrogen oxides in the CNT lattice. The peak maximum at 410.5 eV is the shake-up satellite. Based on the XPS measurements, the nitrogen content of the BCNTs was calculated as 2.66 wt%. The Raman spectra of the N-BCNT sample shows (Figure 2b) a relatively large ratio

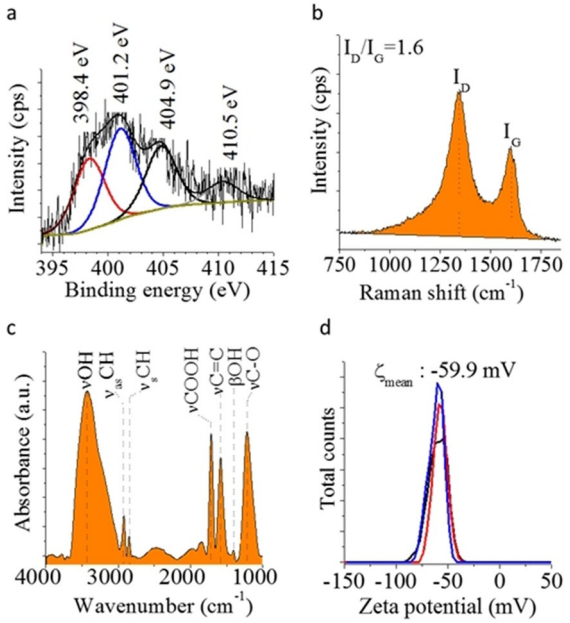

Figure 2. a) Deconvoluted N 1s band on the XPS spectrum and b) Raman spectrum of the BCNTs, c) FTIR results and d) Zeta potential distribution of oxidized BCNTs.

($I_D/I_G = 1.6$); these results indicated a significant number of defects in the graphitic lattice.

After the oxidation of the nanotubes, we studied the forms of oxygen-containing functional groups by infrared spectroscopy on the BCNT surface. Two vibrational bands were evident on the IR spectra, attributed to the carboxy and hydroxyl groups with high intensity (Figure 2c). The absorption bands found in the 3000–3600 cm^{-1} range on the FTIR spectra of the oxidized BCNT samples were assigned to the stretching vibration mode of alcoholic, phenolic and adsorbed water hydroxy (νOH) groups. The absorption for vibrational bands of methylene groups appeared in the 2800–3000 cm^{-1} ($\nu_{as}CH_3$) and 2896–3000 cm^{-1} ($\nu_{as}CH_3$) ranges. The stretching vibration of the carboxy groups were found at ≈1708 cm^{-1}. The absorption peak at around 1577 cm^{-1} can be assumed to be the stretching of C=C bonds in the carbon nanotubes. These bands overlapped often with the C=O stretching vibration band (situated on the FTIR spectrum of the oxidized BCNT as an intensive peak at 1405 cm^{-1} which be attributed to the presence of OH deformation vibration mode βOH). The band at 1216 cm^{-1} can be attributed to the presence of C–O bonds (mainly to esteric, phenolic and alcoholic OH groups.

The number of surface functional groups increased due to the oxidation, so the surface charge density also increased, and that caused a growth in absolute electrokinetic potential values. In case of the proper zeta potential value (oxidized nanotubes: less than −30 mV), the carbon nanotubes are easily dispersible in an aqueous medium and form a stable colloid system. Creating a stable suspension was a necessary step to create calcium alginate–BCNT beads. The measured zeta potential value was −59.9 mV, which satisfies the expected (−30 mV) value (Figure 2d). Based on the zeta potential measurement we can say that the BCNT dispersion in an aqueous phase remains stable.

2.2. Characterization of BCNT Spheres

After the preparation of the gelled BCNT spheres, the BCNT/Ca-alginate grains were carbonized at 1173 K in a nitrogen atmosphere. These BCNT grains were studied by SEM and on the images the surface structures of the BCNT spheres can be observed (Figure 3b). In addition to the nanotubes, carbon layers which cover the nanotubes are visible, indicating that this is a remarkably complex nanosurface.

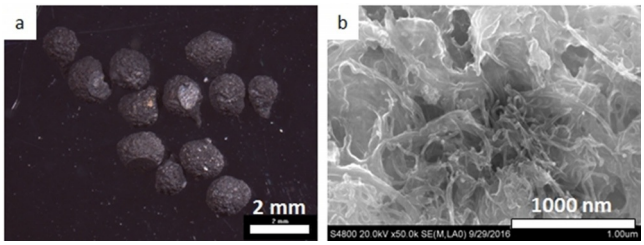

Figure 3. a) Stereomicroscopic photograph and b) SEM image of BCNT spheres.

2.3. Characterization of Pd/BCNT, Ni/BCNT and Rh/BCNT Catalysts

The diameters of catalytically active metal nanoparticles on the surface of Pd-, Rh- and Ni-containing spherical BCNT catalysts was investigated by SEM. The chemical composition of the beads was analyzed by energy-dispersive X-ray spectroscopy (EDS). Based on EDS spectra the metal nanoparticles were identified on the surface of BCNT spheres. The particle diameters of the nanoparticles were also manually scaled using ImageJ program, based on the scale bar.

On the surface of Pd/BCNTs the palladium nanoparticles are clearly visible (Figure 4a). The carbon nanotubes are ruptured by the oxidation step (by HNO_3/H_2SO_4), and the encapsulated Ni were solved; therefore, the nickel peak on the EDS spectrum is not visible (Figure 4a and Figure 4b). The EDS spectrum confirmed the Pd content of the sample. Significant amounts of remaining calcium can be observed in the Pd/BCNTs owing to the preparation of gelled BCNT beads (Figure 4b). The detected Cl is probably derived from the calcium chloride that was used in the gelation process and from the Pd salt (palladium chloro complex) which was used for the decoration of the spheres. The distribution of Pd nanoparticle diameters are heterodisperse (Figure 4c). Based on the results, 80% of Pd nanoparticles had a smaller diameter than 50 nm and the mean diameter was 40.2 nm.

The presence of the metallic phase of the catalytically active metal, namely the palladium, was confirmed by XRD measurement (Figure 4d). On the diffractogram of the catalyst, the Pd (111), Pd (200), Pd (311) and Pd (222) indexed reflections were evident at 40.2, 46.7, 68.2, 82.3 and 86.8 2θ degrees. The reflections peak of BCNTs is visible at 26.1 2θ degree.

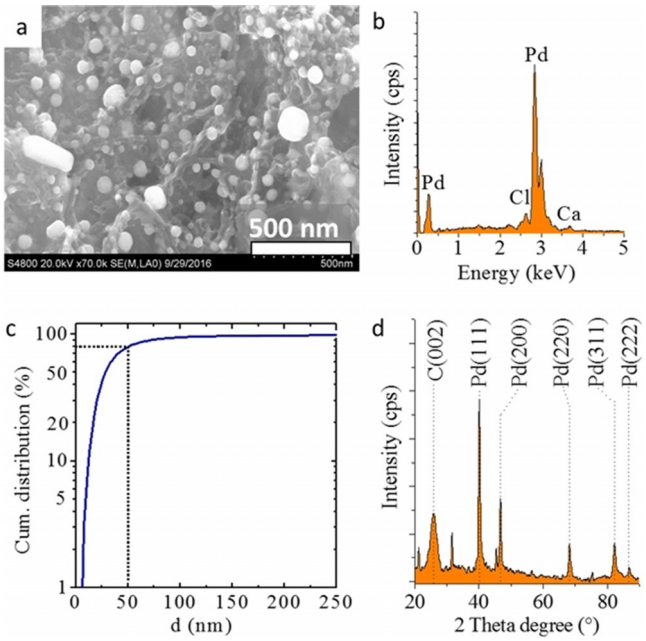

Figure 4. a) SEM image, b) EDS spectrum, c) particle size distribution of the Pd-based system and d) the XRD pattern of the surface of the 5% Pd/BCNT spheres.

The Ni nanoparticles were visible on the surface of the nickel-containing, granulated BCNT catalyst (Figure 5a). Based on the EDS results, the Ca and Cl elements can be attributed to the calcium chloride salt (Figure 5b). The size distribution of Ni nanoparticles was very heterodisperse: The average particle size was 37 nm, the maximum size was 106 nm and minimum particle diameter was 8 nm (Figure 5c). Based on the cumulative size distribution, 80% of Ni nanoparticles had a diameter smaller than 45 nm.

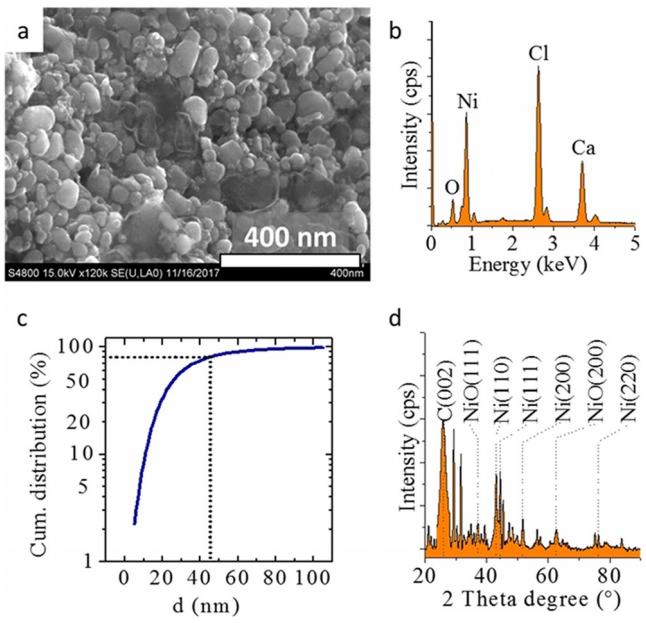

Figure 5. a) SEM image, b) EDS spectrum, c) metal particle size distribution and d) XRD pattern of the 5% Ni/BCNT spheres.

The elemental phases of the nickel were tested by XRD and on the diffractogram the reflection of nickel oxide (111) and (200) planes can be found. The presence of elemental nickel phases (111), (200) and (220) can be identified on the diffractogram (Figure 5d).

On the SEM picture of the Rh/BCNT spherical sample, the nickel particles are of relatively small size (Figure 6a). The EDS result shows the presence of rhodium and calcium. Based on the cumulative size distribution histogram, it can be stated that the average particles size is 7.9 nm, the distribution shows a relatively small scatter: The maximum diameter was 17.8 nm, while the minimum was 3.4 nm (Figure 6c). Based on the results, 80% of Rh nanoparticles had a diameter smaller than 8 nm. On the X-ray diffractogram, the elemental rhodium reflection peaks are evident.

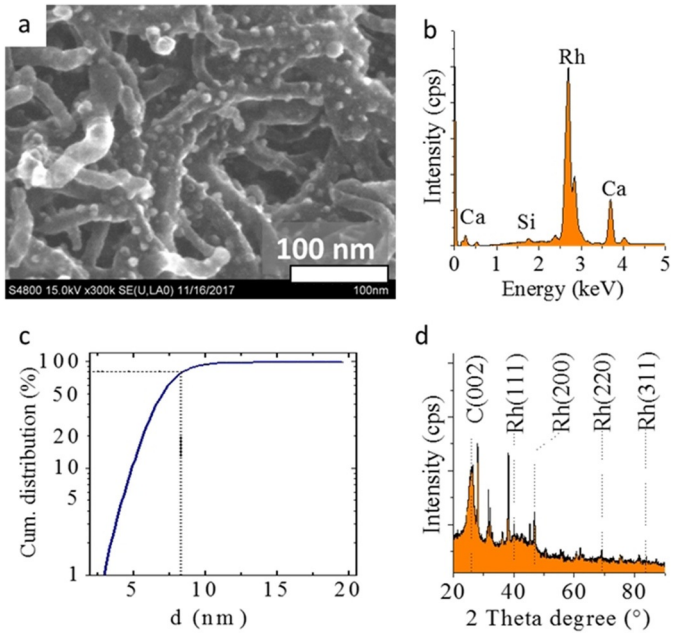

Figure 6. a) SEM image, b) EDS spectrum, c) metal particle size distribution and d) XRD pattern of the 5% Rh/BCNT spheres.

2.4. Catalytic Hydrogenation of CO_2

Ni-, Rh-, and Pd-supported BCNT spheres were tested in CO_2 hydrogenation to form carbon monoxide, methane and ethane (in trace amounts) at 473–873 K in a fix bed flow catalytic reactor and to compare their reactivity. The summarized catalytic results are shown in Figure 7. In the catalytic reaction the major products were CO and methane and a minor amount of C_2 hydrocarbons were also formed. The catalytic measurements in the CO_2 hydrogenation were carried out with stoichiometric ratio of 1:4. The nominal metal content was 5 wt%. The catalytic conversions and the product distributions were determined in the case of the three different catalysts. The conversion of CO_2 was calculated taking into account the amount of carbon dioxide consumed and it was also determined based on the sum carbon balance. Selectivity values were defined as [Eq. (1)]:

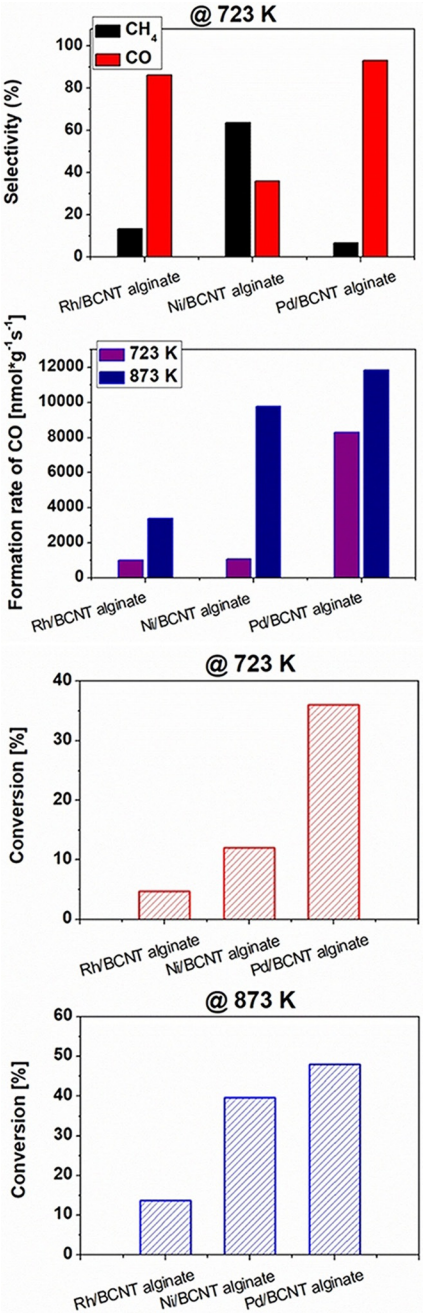

Figure 7. CO_2 hydrogenation over 5% Rh, Ni and Pd BCNT spheres at 723 K and 873 K.

$$S_i = \frac{x_i n_i}{\sum x_i n_i} \quad (1)$$

where x_i *is* the mol fractions of product (i) and n_i is the number of carbon atoms in each molecule of product (i). Experiments were carried out in a temperature range of 473–873 K.

In all cases no appreciable reaction was observed at 473–523 K. The formation of the products appeared first in the experiment at 873 K, and the conversion of CO_2 was about ≈4% in the case of Pd catalyst. When applying the most active 5% Pd/BCNT catalyst, 48% conversion was reached at 873 K. As expected, the CO_2 consumption rate gradually increased with the temperature. With increasing the reaction temperature, the methane selectivity decreased, and the CO selectivity was heavily raised: over 99% was achieved at 873 K. Therefore, we assume that the relative lower temperature is suitable for obtaining high yield of methane.

Firstly, the time on stream was measured at $T = 873$ K (1 bar). As a function of time, at all times the conversion of CO_2 was slightly increased and after that it had reached the highest conversion rate. The final conversion values after 3 h were 26, 38 and 51% in the case of Rh, Ni and Pd catalysts, respectively. These results confirm that all catalysts showed excellent catalytic activity up to at least 3 h.

Based on the time-of-flight results we can observe that the conversion of CO_2 increased with the reaction time in the case of Rh (see Figure S1 in the Supporting Information). This can be explained by the presence or absence of the induction effect on the Rh-based catalyst. The difference in time-on-stream behaviors suggests the possibility of a difference in hydrogen dissociating properties between the support and the metal atoms. When Rh nanoparticles and the support had a common interface so interacted with each other, the H_2 dissociation gets faster and H atoms are surface-diffused and accelerate the reaction. The CO_2 hydrogenation proceeds through the formation of CO, as an intermediate, via the RWGS (reverse water gas shift), followed by CO hydrogenation to methane. The RWGS reaction has been found to take place at the metal–support interface. In our presented work with the Rh and Pd supported on BCNT, the main reaction product is CO. When Rh was deposited on different supports, mainly on reducible TiO_2, methane formation was dominant.[36–39] On Pd-supported Al_2O_3 catalysts, methane formation was dominant,[36–39] whereas using SiO_2, MgO and TiO_2 supports CO was the major product.[37] The ratio of Ni:NiO also strongly determines the selectivity of the CO_2 hydrogenation: higher metallic content favors methane formation.[29] All of these findings emphasize the importance of the nature of the metal/support interface. The absence of an oxide-like interaction between the metal and BCNT could be the reason for high CO selectivity in the present study. The BCNT ensures a spherical, site-specific arrangement for the metal where the CO_2 reductive activation may occur. In the case of Ni/BCNT there is a chance to build up a favorable Ni/NiO composition at a moderate temperature where the methane formation is dominant.

3. Conclusions

In this work, different catalytically active metal nanoparticles were anchored onto the surface of a calcium alginate BCNT support. Rh, Pd and Ni BCNT catalysts were tested in the CO_2 hydrogenation reaction in the gas phase in a flow reactor at 473–873 K. The catalysts were also characterized by TEM, SEM and XRD. Pd/BCNT (5%) was approximately seven and three times more active at 723 K compared with Rh and Ni/BCNT catalysts, respectively.

N-doped BCNTs were synthesized from butylamine by the CCVD method. The nanotubes were functionalized by using a mixture of H_2SO_4/HNO_3. Then, calcium alginate BCNT spheres

were made from the oxidized BCNT, after which time the spherical carbon composites were calcinated. These beads were used as supports for the preparation of palladium-, nickel- and rhodium-containing hydrogenation catalysts. The activity of the BCNT-supported catalysts was tested in CO_2 hydrogenation reactions. Based on these results, we can conclude that the oxide forms of the nickel catalyst promote methane formation. Application of reduced metallic palladium and rhodium does not lead to a greater amount of methane formed, especially at higher temperature. Compared to the two noble metal catalysts, it can be concluded that the application of palladium led to the formation of CO in larger quantities; in this sense the Pd was more efficient than the Rh. A striking difference can be observed between the size distribution of the rhodium and the palladium particles. This difference likely resulted in different catalytic activity during the CO_2 hydrogenation to CO. The formation rate of the CO was higher at 723 K compared to the other two catalysts. Based on these results, we conclude that the final product can be influenced by means of a careful selection of the catalyst. Accordingly, on the Pd/BCNT catalyst the generation of CO was favored and in the case of the Ni/BCNT catalyst, the major pathway was the formation of CH_4. We assume that the surface of the Ni/BCNT catalyst was mainly covered by elemental Ni. However, under the reaction conditions employed, the Ni/NiO_x form was still present which was responsible for the high activity of the catalyst.

Experimental Section

Materials

For the CCVD synthesis the following materials were used: *n*-butylamine (Sigma Aldrich; as the carbon source), $Ni(NO_3)_{2\times}6H_2O$ (Merck) and MgO (Sigma Aldrich) for preparation of CCVD catalyst. The purification of nanotubes was performed with 37 wt% cc. HCl (VWR). Nitric acid, 67 wt% (VWR) and sulfuric acid, 98 wt% (VWR) were used for functionalization of BCNTs. During of application gelled BCNT spheres sodium alginate (Sigma Aldrich) and $CaCl_2$ (Merck) were used. The hydrogenation catalysts were synthetized from the following precursors: $PdCl_2$ (Alfa Aesar), $[(CH_3CO_2)_2Rh]_2$ (Sigma Aldrich), $Ni(NO_3)_{2\times}6H_2O$ (Merck).

Synthesis of N-Doped Carbon Nanotubes

N-doped BCNTs were synthesized from butylamine by a catalytic chemical vapor deposition (CCVD) method. The preparation was performed in a quartz reactor. The nitrogen-containing carbon source (butylamine) was injected into the furnace with an infusion pump. The applied carrier gas was nitrogen and the CNTs were synthesized at 973 K. The reaction took place on a catalyst bed, placed in a quartz-bowl, containing 5 wt% of Ni/MgO catalyst. The desired temperature was controlled by the tube furnace and the sample was positioned in it. After CNT synthesis, the catalyst was removed by boiling the nanotubes in concentrated hydrochloric acid for 6 h. Then the BCNTs were washed with distilled water and dried at 380 K overnight. The purity of the product was checked with thermogravimetric tests (TG).

Functionalization of BCNTs

The nanotubes were functionalized with a mixture of nitric acid and sulfuric acid (1:3 v/v ratio) over 24 h at room temperature with continuous stirring. The samples were washed with distilled water and dried at 380 K overnight. The success of the functionalization was confirmed by Fourier transform infrared spectroscopy (FTIR).

Preparation of Calcium Alginate BCNT Spheres

Two different mixtures were used to prepare calcium alginate BCNT spheres.[35] One of them contained 100 mL distilled water, 1 g Na-alginate and 1 g oxidized BCNT. The other mixture contained 200 mL distilled water and 6 g $CaCl_2$. The Na alginate was dispersed by using a Hielscher homogenizer. Subsequently, using a syringe pump the Na–alginate–BCNT mixture was added dropwise to the $CaCl_2$ solution. During this process the formed beads had the same size as the droplets. After the preparation, the remaining solution was effused, the spheres were washed with distilled water then dried at 350 K for 48 h. The prepared spherically shaped catalyst was calcinated at 1073 K under a nitrogen flow for 20 minutes.

Decoration of Spheres with Pd, Rh and Ni Nanoparticles

The prepared BCNT spheres were impregnated with a palladium chloro complex. 50 mL distilled water was added to 475 mg beads, then 43.1 mg $PdCl_2$ was dissolved in 5 mL distilled water and 1 mL hydrochloric acid with continuous heating. The solution was added to the spheres, and then the water was removed by a rotary evaporator. Finally, the beads were dried at circa 380 K for 12 h and reduced at 673 K in a hydrogen flow. The rhodium-containing catalyst was prepared from 74.3 mg rhodium-acetate dimer $[(CH_3CO_2)_2Rh]_2$ and 657 mg BCNT spheres, similarly to the previous method. In the case of the nickel catalyst, 495 mg $Ni(NO_3)_2$*$6H_2O$ was dissolved in 100 mL distilled water and 1.9 g granulated BCNT was added to the nickel solution. After 30 min agitation, the water was evaporated from the impregnated carbon support and the sample was dried at 380 K. The reduction step was identical to that described previously.

Characterization Techniques

Transmission Electron Microscopy (TEM)

Imaging of the different BCNT supports, metal nanoparticles and derived catalysts were characterized by FEI TECNAI G^2 20 X-Twin high-resolution transmission electron microscope, (equipped with electron diffraction) operating at 200 kV accelerating voltage. The samples were dropcast onto 300 Mesh Copper grids from an aqueous suspension.

Thermogravimetric Measurements (TG)

The purity of the BCNTs was checked by thermogravimetric analysis. The measurements were applied with a MOM Derivatograph-C device, using aluminum oxide as the reference in air. The heat-up rate of the furnace was 5 Kmin^{-1} from ambient temperature up to 1173 K. A differential thermogravimetric curve (DTG) was used to evaluate the TG curve with the MOM WinderC program.

Raman and FTIR Spectroscopy

The structural distortion of BCNTs was examined by WITEC Confocal Raman microscope (alpha 300 R equipped) with a He–Ne laser emitting at $\lambda = 632.95$ nm. The so-called "defect vibration" (D) indicates the deviation from the graphite structure in the Raman spectrum of nanotubes. It typically appears at 1340 cm^{-1}. The vibration of the graphite structure (G) typically occurs at 1590 cm^{-1}. The structural imperfection of carbon nanotubes can be characterized by direct comparison to the I_D/I_G intensity ratios of the above-mentioned vibrations. The chemical nature, namely the oxygen-containing functional groups of the oxidized carbon nanotubes, were examined by FTIR.

X-ray Photoelectron Spectroscopy (XPS)

The forms of incorporated nitrogen atoms in the structure of BCNTs were identified by X-ray photoelectron spectroscopy. The SPECS ultrahigh vacuum (UHV) instrument was equipped with a PHOIBOS 150 series hemispherical electron energy analyzer with an MCD 9 detector, using an Al Kα X-ray radiation source ($h\nu =$ 1486.6 eV). The X-ray gun was operated at 210 W (14 kV, 15 mA). The analyzer was operated in the FAT mode, with the pass energy set to 20 eV.

Zeta Potential Measurements

The study of the stability of the BCNT aqueous dispersion was based on the value of the electrokinetic potential (Zeta potential). The measurement was performed on Nano-ZS, ZetaNanoSizer instrument (Malvern), and a DTS 1070 disposable capillary cell was used. The experiments were based on the laser doppler electrophoresis method.

Scanning Electron Microscopy (SEM)

The imaging of the metal-anchored BCNT spherical catalyst surface was undertaken using a Hitachi S 4800 scanning electron microscopy (SEM) with a Bruker X Flash 4010 EDS analyzer.

Powder X-Ray Diffraction (XRD)

The formation of metallic catalytic nanoparticles (Ni, Rh, Pd) was confirmed by X-ray diffraction measurements. XRD measurement were carried out with a Bruker D8 Advance diffractometer.

Catalytic Activity in the CO_2 Hydrogenation Reaction

Before the catalytic experiments the samples were oxidized in a continuous-flow reactor in O_2 at 573 K for 30 min to remove the contaminants from the surface. Thereafter, they were reduced in a H_2 flow at 573 K for 60 min to reduce the accessible metal particles on the surface.

Catalytic reactions were carried out in a fixed-bed continuous-flow reactor ($D = 10$ mm), which was heated externally by a temperature controller. The dead volume of the reactor was filled with quartz beads. The temperature was controlled by a thermocouple. Under the experiments small fragments ($\approx$1 mm) of lightly compressed pellets were used and the reactor contained $\approx$200 mg of catalyst. In the reacting gas mixture, the CO_2:H_2 molar ratio was 1:4. The CO_2:H_2 mixture was fed with mass flow controller (Area) and the total flow rate was 50 mL min^{-1}. The whole catalytic system was covered by an externally heated tube to avoid condensation. The analysis of the products and reactants was performed with a HP 4890 gas chromatograph using Equity-1 capillary and Porapak Q + Porapak S packed columns to allow the complete separation. The gases were detected by thermal conductivity (TCD) and flame ionization (FID) detectors.

In a typical experiment after the pre-treatment, the sample was cooled down in an inert carrier gas (Ar) to the lowest reaction temperature (473 K). The catalyst was introduced into a CO_2:H_2 mixture with a molar ratio of 1:4 with a total flow rate of 50 mL min^{-1}. From 473 K the reactor was heated up to the next evaluation temperature and, after the final set point (873 K), equilibrated for 200 min to check the stability of the catalysts as a function of time.

Acknowledgements

The project was supported through the New National Excellence Program of the Ministry of Human Capacities. This work was supported by the Ministry of the Hungarian Research Development and Innovation Office through grants NKFIH OTKA PD 115769, OTKA 128543 and OTKA K120115. This research was supported by the European Union and the Hungarian State, co-financed by the European Regional Development Fund in the framework of the GINOP-2.3.4–15–2016-00004 project, aimed to promote the cooperation between the higher education and the industry. The research was also supported by the GINOP-2.3.2–15–2016-00013 project.

Conflict of Interest

The authors declare no conflict of interest.

Keywords: carbon nanotubes · chemical vapor deposition · CO_2 hydrogenation · methane formation · supported catalysts

[1] P. G. Collins, M. S. Arnold, P. Avouris, *Science* **2001**, *292*, 706–709.
[2] R. M. Falvo, C. J. Clary, R. M. Taylor, V. Chi, F. P. Brooks, S. Washburn, R. Superfine, *Nature* **1997**, *389*, 582–584.
[3] B. I. Yakabson, R. E. Smalley, *Am. Sci.* **1997**, *85*, 324–337.
[4] R. S. Rouff, D. C. Lorents, *Carbon* **1995**, *33*, 925–930.
[5] C. Klinger, Y. Patel, H. W. C. Postma, *PLoS ONE* **2012**, *7*, 37806.
[6] T. Dürkop, S. A. Getty, E. Cobas, M. S. Fuhrer, *Nano Lett.* **2004**, *4*, 35–39.
[7] J. B. Cui, R. Sordan, M. Burghard, K. Kern, *Appl. Phys. Lett.* **2002**, *81*, 3260.
[8] P. J. F. Harris, *Int. Mater. Rev.* **2004**, *49*, 31–43.
[9] T. Yamamoto, K. Kawaguchi, *Colloids Surf. A* **2017**, *529*, 765–770.
[10] Z. Akram, A. Kausar, M. Siddiq, *Polym.-Plast. Technol. Eng.* **2016**, *55*, 582–603.
[11] I. Hasanzadeh, A. R. Mahdavian, M. Barikani, *Eur. Polym. J.* **2016**, *75*, 104–115.
[12] M. Kanellos, **2006**, https://www.cnet.com/news/carbon-nanotubes-enter-tour-de-france/ Accessed 1 September **2017**.
[13] S. Farzada, A. Rashidib, M. A. Haghtalabc, *Fuel* **2014**, *132*, 27–35.
[14] M. S. Mauter, M. Elimelech, *Environ. Sci. Technol.* **2008**, *42*, 5843–5859.
[15] J. Kang, X. Duan, C. Wang, H. Sun, X. Tan, M. O. Tade, S. Wang, *Chem. Eng. J.* **2018**, *332*, 398–408.
[16] L. Xiaoshu, X. Jiang, J. Guangming, X. Xinhua, *Chemosphere* **2011**, *85*, 1204–1209.
[17] R. Wang, T. Yan, L. Han, G. Chen, H. Li, J. Zhang, L. Shi, D. Zhang, *J. Mater. Chem. A* **2018**, *6*, 5752–5761.
[18] H. G. Liao, Y. J. Xiao, H. K. Zhang, P. L. Liu, K. Y. You, C. Hean, W. Luo, *Catal. Commun.* **2012**, *19*, 80–84.

[19] L. Vanyorek, Gy. Halasi, P. Pekker, F. Kristály, Z. Kónya, *Catal. Lett.* **2016**, *146*, 2268 – 2277.
[20] L. Vanyorek, F. Kristály, A. Mihalkó, O. Bánhidi, Á. Kukovecz, Z. Kónya, J. Lakatos, *Reac. Kinet. Mech. Kat.* **2015**, *116*, 371 – 383.
[21] Y. H. Li, T. H. Hung, Y. H. Chen, *Carbon* **2009**, *47*, 850 – 855.
[22] J. Zhang, J. Fang, J. Han, T. Yan, L. Shi, D. Zhang, *J. Mater. Chem. A* **2018**, *6*, 15245 – 15252.
[23] L. Yan, D. Li, T. Yan, G. Chen, L. Shi, Z. An, D. Zhang, *ACS Sustain. Chem. Eng.* **2018**, *6*, 5265 – 5272.
[24] P. Ayala, R. Arenal, M. Rümmeli, A. Rubio, T. Pichler, *Carbon* **2010**, *48*, 575 – 586.
[25] P. Gao, S. Li, X. Bu, S. Dang, Z. Liu, H. Wang, L. Zhong, M. Qiu, C. Yang, J. Cai, W. Wei, Y. Sun, *Nat. Chem.* **2017**, 9, 1019 – 1024.
[26] H. Song, N. Zhang, C. Zhong, Z. Liu, M. Xiao, H. Gai, *New J. Chem.* **2017**, *41*, 9170 – 9177.
[27] H. Bahruji, M. Bowker, G. Hutchings, N. D. P. Wells, E. Gibson, W. Jones, C. Brookes, D. Morgan, G. Lalev, *J. Catal.* **2016**, *343*, 133 – 146.
[28] S. Bai, Q. Shao, P. Wang, Q. Dai, X. Wang, X. Huang, *J. Am. Chem. Soc.* **2017**, *139*, 6827 – 6830.
[29] A. Sápi, Gy. Halasi, J. Kiss, D. Dobó, L. K. Juhász, J. V. Kolcsár, Zs. Ferencz, G. Vári, V. Matolin, A. Erdőhelyi, Á. Kukovecz, Z. Kónya, *J. Phys. Chem. C* **2018**, *122*, 5553 – 5565.
[30] S. K. Beaumont, S. Alayoglu, C. Specht, W. D. Michalak, V. V. Pushkarev, J. Guo, N. Kruse, G. A. Somorjai, *J. Am. Chem. Soc.* **2014**, *136*, 9898 – 9901.
[31] A. Sápi, A. Varga, G. F. Samu, D. G. Dobó, K. L. Juhász, B. Takacs, E. Varga, A. Kukovecz, Z. Kónya, C. Janáky, *J. Phys. Chem. C* **2017**, *121*, 12148 – 12158.
[32] Gy. Halasi, A. Gazsi, T. Bánsági, F. Solymosi, *Appl. Catal. A* **2015**, *506*, 85 – 90.
[33] F. Solymosi, A. Erdőhelyi, T. Bánsági, *J. Chem. Soc. Faraday Trans. 1* **1981**, *77*, 2645 – 2657.
[34] C.-S. Li, G. Melaet, W. T. Ralston, K. An, C. Brooks, Y. Ye, Y.-S. Liu, J. Zhu, J. Guo, S. Alayoglu, G. A. Somorjai, *Nat. Commun.* **2015**, *6*, 6538.
[35] H. Ba, C. Duong-Viet, Y. Liu, J.-M. Nhut, P. Granger, M. J. Ledoux, C. Pham-Huu, *Comptes Rendus Chim.* **2016**, *19*, 1303 – 1309.
[36] É. Novák, K. Fodor, T. Szailer, A. Oszkó, A. Erdőhelyi, *Top. Catal.* **2002**, *20*, 107 – 117.
[37] A. Erdőhelyi, M. Pásztor, F. Solymosi, *J. Catal.* **1986**, *98*, 166 – 177.
[38] X. Wang, H. Shi, J. H. Kwak, J. Szanyi, *ACS Catal.* **2015**, *5*, 6337 – 6349.
[39] X. Wang, H. Shi, J. Szanyi, *Nat. Commun.* **2017**, *8*, 513.

Received: August 7, 2018
Revised manuscript received: August 28, 2018

